ACS Sustainable Chemistry & Engineering

Research Article

pubs.acs.org/journal/ascecg

Tailored Structure and Properties of Injection-Molded Atactic Polypropylene/Isotactic Polypropylene Blend

Zhengchi Zhang,[†] Jun Lei,*[,†] Yanhui Chen,[†] Jun Chen,[†] Xu Ji,[‡] Jianhua Tang,[†] and Zhong-Ming Li*[,†]

[†]College of Polymer Science and Engineering, State Key Laboratory of Polymer Materials Engineering, Sichuan University, Chengdu 610065, China

[‡]College of Chemical Engineering, Sichuan University, Chengdu 610065, China

ABSTRACT: In the present work, atactic polypropylene (aPP)/isotactic polypropylene (iPP) with different aPP content was prepared through an injection-molding process to improve the toughness of iPP and make large scale use of aPP. The hierarchic structure of the injection-molded parts was characterized through differential scanning calorimetry (DSC), wide-angle X-ray diffraction (WAXD), small-angle X-ray scattering (SAXS), and scanning electron microscopy (SEM). It was found that the network of iPP crystals was still integral with shish-kebab structures in the skin layer and the relatively high crystallinity of iPP in injection-molded parts with low aPP content utilizing suitable process conditions. Therefore, the toughness of iPP was enhanced from 31.8 to 42.6 MJ/m^3 due to the addition of a 20 wt % aPP component, meanwhile the tensile strength only decreased from 45.9 to 40.5 MPa. Furthermore, when aPP content reached 50 wt %, the toughness of the aPP/iPP blends increased to 52.0 MJ/m^3 with the tensile strength staying at the level of 20 MPa, indicating that the A50 sample also has good toughness with reasonable strength. The results demonstrated that the aPP/iPP blends with high mechanical properties owing to the optimized inner structure can be obtained through the suitable processing method. Our results set up a new method to make large scale use of aPP. Moreover, with an increase in aPP content, the mechanical properties of the injection-molded part can be divided into three evolution stages with distinct differences. At high and low aPP content, the mechanical properties were not sensitive to aPP content. However, when aPP content fell between 20 and 50 wt %, the mechanical properties of the injection-molded part, especially the elongation at the break, changed dramatically acting like percolation phenomenon in electro-conductive polymer composites, which may be the result of phase inversion of aPP/iPP blends. The percolation in mechanical properties is meaningful to prepare the blend of crystallizable/noncrystallizable blends with different properties.

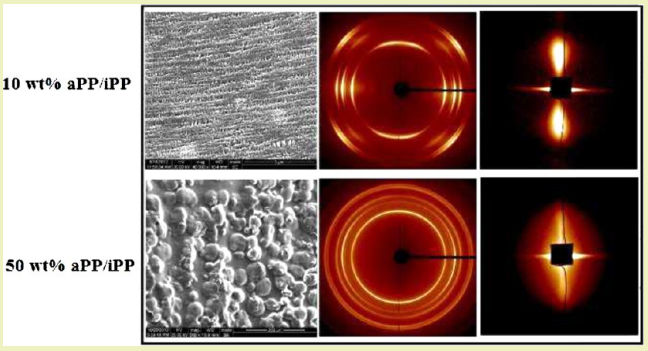

KEYWORDS: *Atactic polypropylene, Isotactic polypropylene, Injection molding, Mechanical properties, Percolation phenomenon*

INTRODUCTION

Atactic polypropylene (aPP) is a general noncrystalline byproduct of propylene polymerization with a global output of about 1−2.5 million tons per year accounting for 2−5% of the production of polypropylene, which is often regarded as inevitable industry waste with limited application (mainly, fuels, adhesives, and coatings). It is undoubtedly an enormous waste of oil resources that aPP is consumed in these inefficient and low value-added usages. For this reason, how to use aPP effectively becomes an important issue.

aPP behaves like liquid oil, either a soft viscous solid with increasing molecular weight and or a gum elastomer at room temperature with proper molecular weight,[1] which has the potential to toughen polymers at ambient temperature and above.[2] Hereby, it is natural to consider toughening iPP with blending aPP due to their good compatibility and the very low price of aPP. As reported by K. Friedrich, the impact strength of iPP at room temperature improved with an increase in atactic content; unfortunately, it is also accompanied by an observable decrease in yield strength and shear modulus due to the poor mechanical properties of aPP.[3] In this case, many researches basically focus on the theoretical problems of aPP/iPP blends, for example, the influence of temperature on the phase behavior of aPP/iPP blends. The aPP component was reported to be miscible with iPP in the molten state from the evaluation of an equation of state theory when aPP content is low,[4,5] which makes it easy to mix aPP and iPP to obtain uniform blends. However, some research results argued that the miscibility of aPP and iPP is sensitive to temperature. The experiments of Keith and Padden demonstrated that aPP and iPP have good compatibility under high temperature, yet when the temperature is lower than the crystallization temperature of iPP, phase separation happens.[6] This is consistent with the simulation results obtained by Choi and Mattice.[7] Phillips reported that at high crystallization undercooling, the rapid crystallization of iPP

Received: February 8, 2013
Published: May 30, 2013

would obscure the underlying phase behavior of the weakly interacting iPP/aPP pair. Oppositely, low undercooling revealed the underlying phase behavior as a nodular texture within the aPP/iPP spherulite.[8] Through time-resolved X-ray scattering techniques, the results reported by Wang et al. showed relatively modest incorporation of aPP in the interlamellar regions depending on the crystallization temperature and composition of blend.[9] It is reasonable to deduce that the final morphology of aPP/iPP blends is governed by the phase separation process resulting from iPP crystallization. Therefore, it is interesting and necessary to determine how the final phase and crystal morphology of aPP/iPP blends affect the properties.

Another important factor for aPP/iPP blend is the aPP content, which will affect not only the miscibility and phase behavior of aPP and iPP but also the crystallization of iPP, hence the properties of aPP/iPP blends. Keith et al.'s results showed that with increasing aPP concentration, a more open spherulitic texture was produced because of the incorporation of aPP diluents in the interfibrillar regions.[10] Analogously, Wang et al. reported that with a large amount of aPP, a decrease in crystallinity of aPP/iPP blends should be attributed to the large amount of aPP diluents, which suppressed the concentration of the nucleus and reduced iPP molecular diffusion to the surface of nucleus during crystallization.[9]

All these studies mentioned above laid particular emphases on the phase behavior and morphology of aPP/iPP blends. Limited research has paid attention to the mechanical performance of aPP/iPP blends, which is determined by the phase and crystallization morphology.[11] Wenig and Schöller reported that the elastic modulus, yield stress, and stress at break of aPP/iPP blends decreased observably with an increase in aPP content.[12] Through adjusting the external fields in processing to obtain specific phase and crystal morphology, it can be expected that the mechanical properties of aPP/iPP blends will be improved. However, the phase and crystal morphology of aPP/iPP blends in practical injection molding, one of the most widely used processing methods, has not been studied yet.

In this work, we focused on the effect of aPP content on the mechanical properties of injection-molded aPP/iPP blends with high aPP content in order to make full use of aPP with a premise of accepted properties. For the purpose of overcoming the suppression of aPP in mechanical properties and preparing aPP/iPP blends with desired mechanical properties, an injection mold with a hot runner was employed in this work; in the mean time, high mold temperature was set during processing. They both resulted in slow solidifying of the melt in cavity and long packing time. Employing this processing method, aPP/iPP blends with high aPP content were fabricated. After characterizing phase morphology, iPP crystallinity in the blend using wide-angle X-ray diffraction (WAXD), small-angle X-ray scattering (SAXS), differential scanning calorimetry (DSC), and scanning electronic microscopy (SEM), we evaluated the mechanical properties of aPP/iPP blends and proposed the deformation mechanism during tensile test before and after phase inversion. Moreover, the "percolation-like" behavior of mechanical properties of aPP/iPP blends with different aPP contents was put forward, which may help understand the toughening of iPP with a large amount of aPP.

EXPERIMENTAL SECTION

Materials. The iPP (S1003) used in this work was purchased from Dushanzi Petroleum Chemical Co. (China) with a melt flow rate (MFR) of 3 g/10 min (230 °C, 21.6 N), M_w of 39.9×10^4 g/mol, and M_w/M_n = 4.6. The aPP, whose trade mark is 399, is a commercial product of Exxon Mobil, which performs like an elastomer at ambient temperature because its $M_w = 5.2 \times 10^4$ g/mol, and M_w/M_n = 4.1. Solvent extraction was employed to measure the stereoregularity of aPP and iPP. The stereoregularity of iPP is about 98% and that of aPP is 0 after 6 h extraction, indicating there is almost no isotactic component in aPP used in our work.

Sample Preparation. The iPP and aPP were melt mixed by using a twin-screw extruder with a temperature profile of 120, 160, 180, 180, 180, and 180 °C from hopper to die. The blended pellets were injection-molded into dumbbell bars after being fully dried, and the details of injection molding will be described next. Six different series of samples have been prepared for this research. They are denoted as A0, A10, A20, A30, A50, and A70, where the numbers indicate the percent weight content of aPP in the blends.

Injection Molding. The temperature profile for injection molding was 120, 180, 200, 200, and 190 °C from hopper to nozzle. The temperatures of the hot runner were 180, 180, 175, 175, 170, and 165 °C for A0, A10, A20, A30, A50, and A70, respectively. Here, the change of hot runner temperature for different blends is to accommodate their different melt viscosities. For all blends, the mold temperature, packing time, and packing pressure were the same, i.e., 40 °C, 180 s, and 60 MPa, respectively.

Tensile Tests. Tensile tests were performed at room temperature (about 23 °C) using an Instron universal tensile testing machine with a crosshead speed of 50 mm/min according to the ASTMD-638 standard. The tensile properties were obtained by averaging the values of at least five samples. Furthermore, using the area under the stress–strain curve, we can acquire information on the toughness or the energy absorbed by the bulk before breaking (breaking energy).

DSC Analysis. Thermal behaviors of all blends were measured with a differential scanning calorimeter (TA DSC Q200). The samples of about 5 mg cut from different layers of injection-molded bars were first heated from 80 to 200 °C at a rate of 10 °C/min under a nitrogen atmosphere; then, the melting thermograms were measured. The temperature and area of the endothermic peak were taken as the melting peak temperature (T_{mp}) and the heat of fusion (ΔH_f), respectively. For isothermal crystallization, the samples with different content of aPP were first melted at 200 °C for 3 min to eliminate any thermal history and then were cooled to 80 °C at a constant rate of 10 °C/min under a nitrogen atmosphere. The data were collected from 180 to 80 °C.

The theoretical formula of melting enthalpy can be expressed as $\Delta H_f = \Delta H_f^{aPP} \times X_\omega\ \Delta H_f^\circ \times (1 - X_\omega) \times X_c$, where, ΔH_f, ΔH_f^{aPP}, ΔH_f°, X_ω, and X_c are the melting enthalpy of aPP/iPP blend, melting enthalpy of pure aPP, standard melting enthalpy of iPP, mass content of aPP, and crystallinity of iPP. As a kind of amorphous polymer, the melting enthalpy of aPP (ΔH_f^{aPP}) is usually considered to be zero. However, ΔH_f^{aPP} is 9.00 J/g under the heating rate of 10 °C/min, which may come from the melting of extremely little content of iPP in commercial aPP used in our work. The ΔH_f° is 209 J/g for iPP α phase.[13] Therefore, X_c can be calculated using the formula above.

X-ray Diffraction Measurement. Two-dimensional X-ray wide-angle diffraction (2D-WAXD) and small-angle X-ray scattering (2D-SAXS) were carried out at the beamline BL15U1 and BL16B1 of Shanghai Synchrotron Radiation Facility (SSRF, Shanghai, China), respectively. For 2D-WAXD measurements, the monochromatic X-ray beam with a wavelength of 0.1371 nm was focused to 3 μm × 2.7 μm, and the distance from sample to detector was 147.5 mm. The 2D-WAXD images were collected with an X-ray CCD detector (Model SX165, Rayonix Co. Ltd., America). For 2D-SAXS measurements, the X-ray with a wavelength of 0.1371 nm was focused to 300 μm × 500 μm, and the 2D-SAXS images were collected with an X-ray CCD detector (Model Mar165, 2048 × 2048 pixels of 80 μm × 80 μm). The sample-to-detector distance was held at 1900 mm.

The samples for WAXD and SAXS measurement were machined from the 6 mm wide and 4.0 mm thick tensile bar to a 1 mm wide and 4.0 mm thick piece, and the samples obtained were the middle section of the tensile bar, detailed preparation information can refer to Chen et al.'s work.[14] Figure 1 is the schematic diagram of the positions of the samples for WAXD measurement. The direction normal to MD−TD (molding direction−transverse direction) plane was defined as ND, and the X-ray beam was perpendicular to MD−TD plane. Six locations [0 and 600 μm (skin layer), 1200 and 1800 μm (intermediate layer), and 2400 and 3000 μm (core layer) (center circle of the X-ray beam)] down from the MD−TD surface were scanned, respectively.

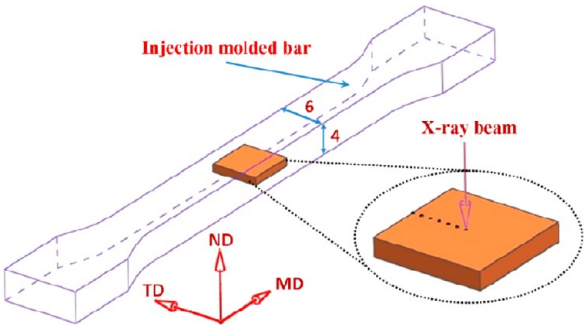

Figure 1. Schematic diagram of the positions of the sample for WAXD measurement.

WAXD and SAXS Data Analysis. 2D-WAXS patterns were analyzed using the Fit-2D software and 1D-WAXD profiles were obtained from circularly integrated intensities of 2D-WAXD image patterns acquired.

The degree of orientation of the developing lamellar structures was estimated from the value of the Hermans orientation factor (f_H),

$$f_H = \frac{1}{2}(3\cos^2\varphi - 1) \quad (1)$$

where $\cos^2\varphi$ is the average cosine squared of the angle between the perpendicular to the scatterers (lamellar stacks) and the flow direction and is given by

$$\cos^2\varphi = \frac{\int_0^{\pi/2} I(\theta)\cos^2\theta \sin\theta d\theta}{\int_0^{\pi/2} I(\theta)\sin\theta d\theta} \quad (2)$$

with θ representing the azimuthal angle in the diffraction pattern.

To calculate the Hermans orientation factor, the angular variation of the intensity was extracted from the 2D-SAXS data through an azimuthal scan ($I(\theta)$), obtained by averaging the intensity over a small q region centered around the value of the peak in the radial intensity profile. The orientation function f_H = 1 when the probed axis is perfectly parallel to the reference direction, f_H = −0.5 when the probed axis is perfectly perpendicular to the reference direction, and f_H = 0 when the probed axis is randomly distributed.

SEM. Permanganic etching was used for the sample surface for observation as described by Bassett et al.[15] The surfaces of all the samples were sputter-coated with a layer of gold to provide enhanced conductivity. Then the morphology was observed in a field emission SEM (Inspect-F, Fei, Finland), operating at 20 kV.

POM. The optical morphologies of all blends were investigated with a polarized optical microscope (Olympus BX-51, with a Linkman CSS450 hot stage). The samples, inserted between two microscope cover glasses, were prepared by solution blending. Each sample was melted at 200 °C for 5 min to eliminate any previous thermal history; they were then cooled to isothermal 141 °C at a rate of 30 °C/min and maintained at this temperature for the time necessary for crystallization. The distance between the two microscope cover glasses is 10 μm. The polymer melt was subjected to shear immediately after the temperature dropped to 141 °C. A shear rate of 10 s^{-1} and shear durations, t_s = 30 s, were selected. POM images were collected continuously before, during, and after cessation of shear.

RESULTS

Crystalline Structure. Figure 2 shows a series of WAXD patterns from different layers, viz., skin, intermediate, and core

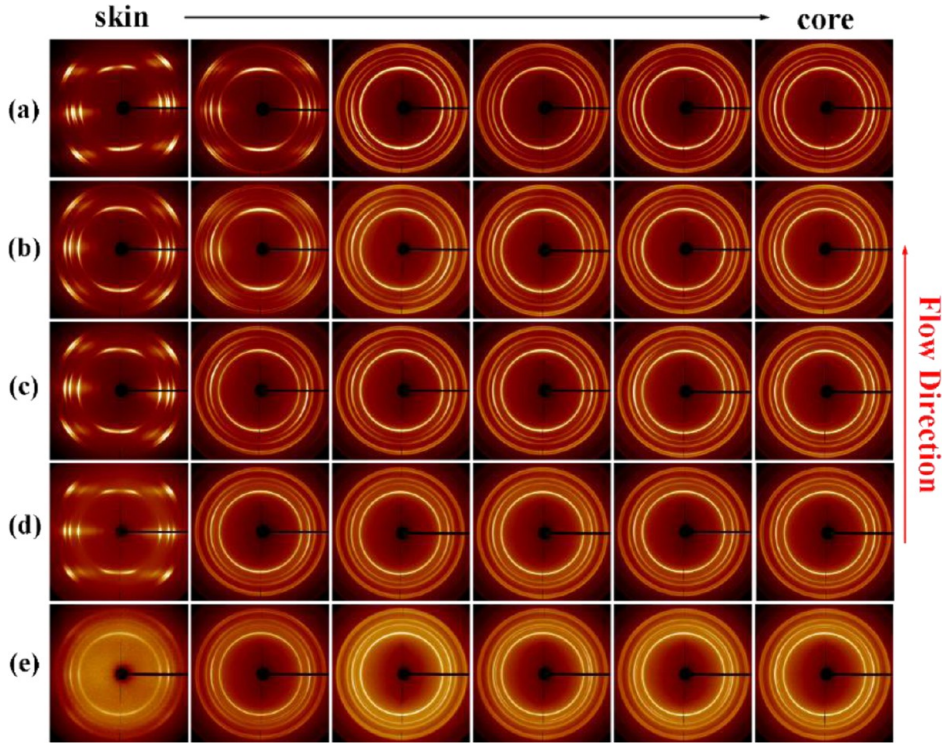

Figure 2. 2D-WAXD patterns of samples with different contents of aPP: (a) A0, (b) A10, (c) A20, (d) A50, and (e) A70.

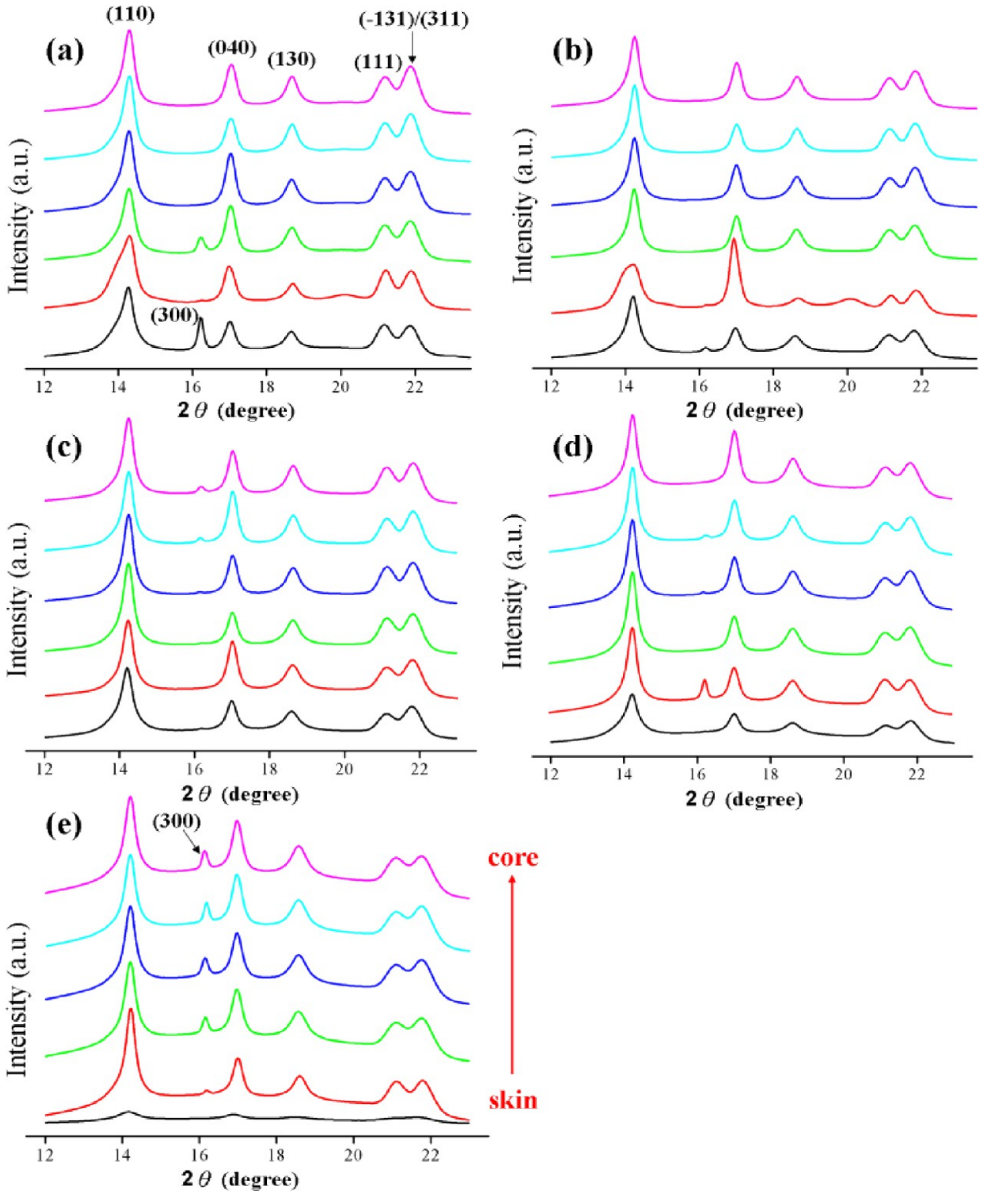

Figure 3. 1D-WAXD curves of samples of (a) A0, (b) A10, (c) A20, (d) A50, and (e) A70 obtained from circularly integrated intensities of 2D-WAXD patterns.

layer. The diffraction patterns of WAXD only show the crystal information of iPP in blends because aPP is a kind of amorphous polymer, and its chain segments are not likely to be incorporated in the iPP nuclei or crystal due to the stringent requirement of the crystal stem concerning the pending CH_3 groups.[16] In every layer of injection sample, the diffraction intensity distribution basically consists of five diffraction rings associated with different lattice planes of iPP, including (110), (040), (130), (111), and (−131), from inner to outer circles, respectively, which are typical of α-crystals. An additional shallow (300) lattice plane appears in the skin layer of A0 and A50 (Figure 2a,d) and every layer of A70 (Figure 2e) corresponding to the reflection of β-crystals.

After circularly integrating intensities of WAXD patterns, 1D-WAXD curves of samples with different aPP contents are present in Figure 3. It is clearly shown that the iPP component in aPP/iPP blends exhibits mainly α-crystals in the bulk of injection-molded parts, while only a little amount of β-crystals appears in the skin layers of A0 and A50 (Figure 3a,d) and every layer of A70 (Figure 3e). During injection processing, when iPP melt flows along the mold wall, the shear flow emerges due to velocity gradient, which makes the iPP melt orient (The oriented crystalline structures of injection-molded parts will be discussed in detail in later parts of this paper.). The oriented melt contacting the cold mold is frozen and persisted due to fast cooling. Meanwhile, the formation of some β-crystals in iPP is induced by the surface of α-row-nuclei generated by the oriented iPP melt.[17] Therefore, the appearance of β-crystals and the molecular orientation in the skin layer are the reasonable results. The reason why β-crystals appear in every layer of injection-molded parts with 70 wt % aPP content (Figure 3e) is not clear for now. Because iPP shows typical α-crystals in aPP/iPP blends with all aPP contents used in our experiment, aPP barely has an impact on the crystal form of iPP. This result is in agreement with the work reported by Lohse et al., which demonstrated that the lattice parameters of the iPP crystals were unchanged upon blending with aPP.[18] In addition, as shown in Figure 2, the

dx.doi.org/10.1021/sc400140y | ACS Sustainable Chem. Eng. 2013, 1, 937−949

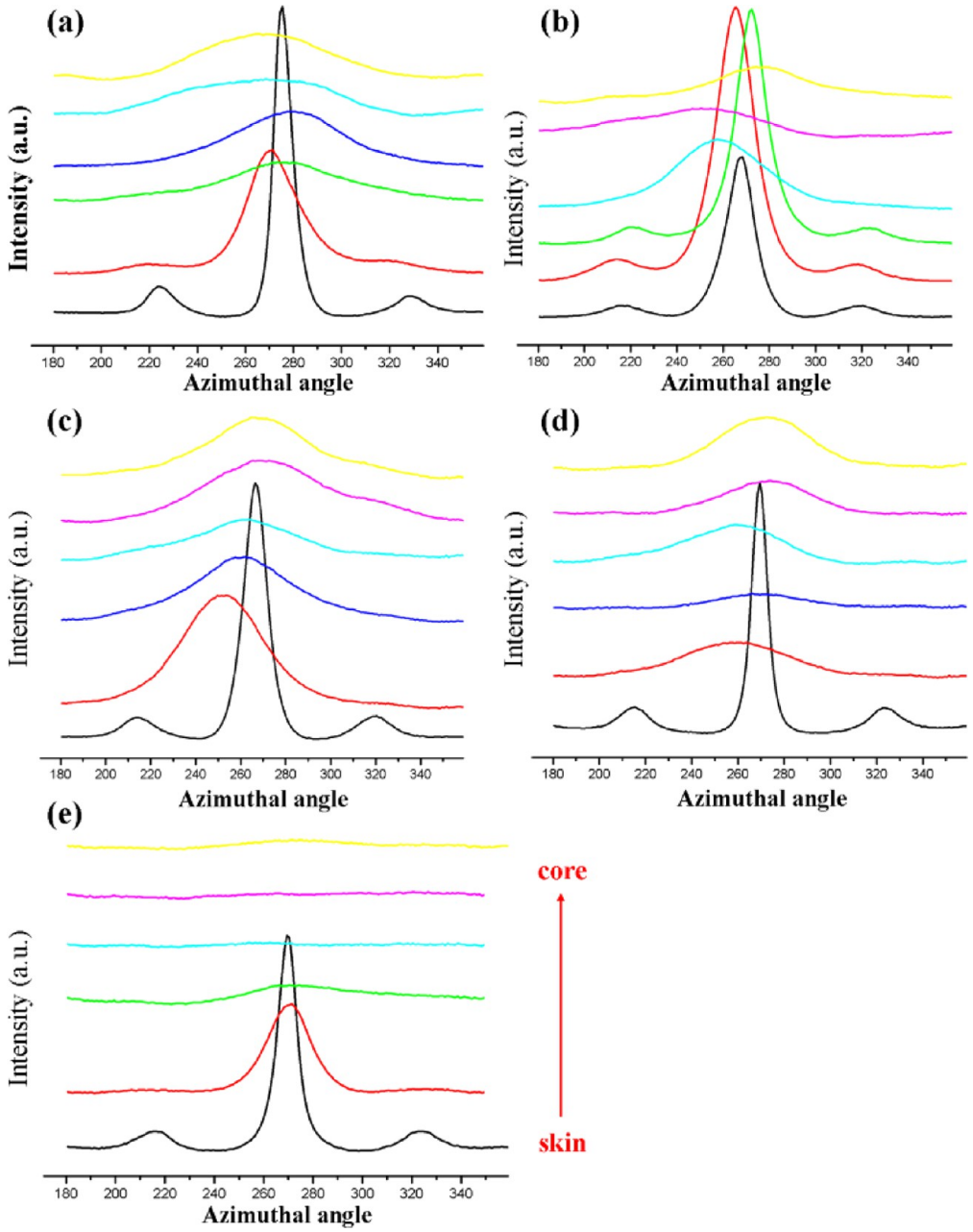

Figure 4. Intensity distribution of $\alpha(040)$ along azimuthal angle of samples of (a) A0, (b) A10, (c) A20, (d) A50, and (e) A70.

diffraction rings of iPP crystals become fuzzy with an increase in aPP content due to a decrease in the crystallizable iPP component. This is more clearly observed from the 1D-WAXD curve in the skin layer of A70 where there is only very weak diffraction peaks (Figure 3e) as a result of high aPP content.

The variation in the intensity of crystal reflections as a function of azimuthal angle is an indication of crystalline orientation. The arc-like diffractions in the skin layer's patterns of aPP/iPP blends clearly suggest the molecular orientation of iPP, which results from the shear flow on the mold wall. This result is confirmed by the narrow peaks in the azimuthal profiles of the skin layers as shown in Figure 4. In addition, two additional peaks appear in the off-axial degree in the skin layers of all samples, which may indicate the presence of $\gamma(008)$ crystal plane. With moving from skin to core of injection-molded parts, the intensity distribution of $\alpha(040)$ along the azimuthal angle changes from narrow to broad. Although the melt in the core layer is also subjected to shear flow, the slow solidifying rate leaves enough time to relax back to random coils for extended iPP chains, and as a result, iPP crystallizes into isotropic α-crystals, which shows uniform diffraction rings in the WAXD patterns (core layers of Figure 2). In other words, the injection-molded parts of aPP/iPP blends exhibit typical skin−core structure with highly oriented skin layers and relatively isotropic core layers.

As shown in the WAXD patterns (Figure 2) and azimuthal profiles (Figure 4), with an increase in aPP content, the orientation of iPP crystals becomes weak in the same position of injection-molded parts with a fixed position of diffraction rings, i.e., the 2θ angles of scattering peaks indicative of the lattice parameters of iPP crystals are not disturbed by the aPP component (Figure 3). At a low aPP content, i.e., A10 and A20, the WAXD patterns are similar to A0, which is also confirmed by azimuthal profiles as shown in Figure 4a−c. When aPP

dx.doi.org/10.1021/sc400140y | ACS Sustainable Chem. Eng. 2013, 1, 937−949

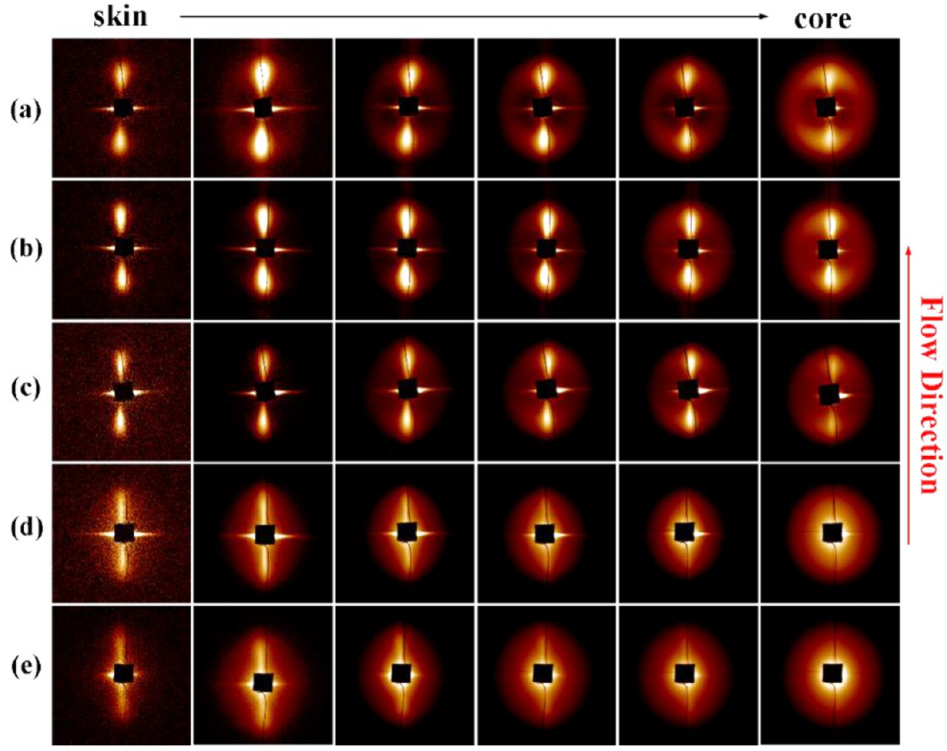

Figure 5. 2D-SAXS patterns of samples with different contents of aPP (a) A0, (b) A10, (c) A20, (d) A50, and (e) A70.

content reaches 50 wt %, the intensity distribution of $\alpha(040)$ of the intermediate layer is broader than that of A20, as shown in Figure 4d. When the aPP content exceeds 50 wt %, i.e., A70, the diffraction rings become isotropic (Figure 2e) and the azimuthal profiles turn flat (Figure 4e) in the injection-molded part, suggesting a lack of oriented iPP crystals, except for the skin layer that has only very weak orientation. With an increase in aPP content, the position where the oriented iPP crystals emerge gets closer to the surface layer of injection-molded parts. In other words, higher shear rate is needed for the formation of oriented iPP crystals at high aPP content, indicating that the presence of aPP is an adverse factor in formation of oriented structure.

Oriented Structure. The lamellar orientation of aPP/iPP blends was further characterized by SAXS, as shown in Figure 5. The Hermans orientation factor (f_H) of iPP/aPP blends with different aPP contents along the direction parallel to flow direction is shown in Figure 6. Normally, the scattering streaks normal to flow direction represent shishes, while the scattering maxima along the flow direction represent kebabs. It can be observed that the scattering maxima along the flow direction change from narrow to broad orientation from the skin to core layer for neat iPP and all blends, which demonstrates a gradual decrease in the lamellar orientation from the skin to core layer. The oriented structure, i.e., shish-kebab, is observed in the skin layers of all samples. Moving toward the core layer, the SAXS patterns become more and more isotropic, especially in the core layers of A50 and A70 (Figure 5d,e). This result is further confirmed by f_H (shown in Figure 6). The f_H of all blends with different aPP contents exhibits a monotonically declined tendency except the surface layer. Because of the size of the X-ray beam (300 μm × 500 μm), only a part of the X-ray beam was focused on the sample when the SAXS pattern of skin layer was collected, which may result in the relatively low f_H. When melt was injected into the mold, the melt close to the mold wall

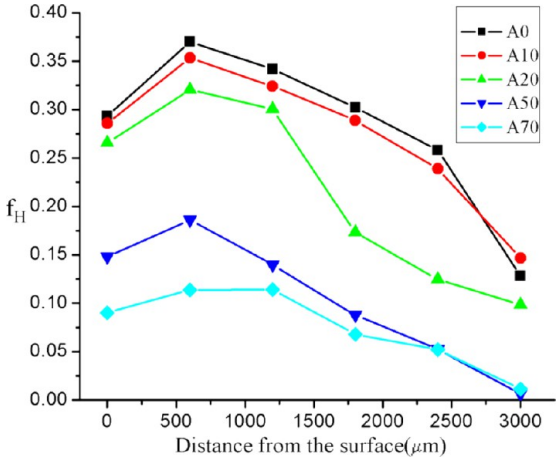

Figure 6. Hermans orientation factor (f_H) of samples with different aPP contents along the direction perpendicular to flow direction.

was subjected to the highest shear rate and immediately cooled by the mold wall. A higher shear rate and/or higher stress lead to a higher orientation of molecular chains, while a faster cooling rate slows down the relaxation or even freezes the orientation by the kick-in of crystallization. A combination of high shear stress and low temperature generated a high orientation of crystals in the skin layer leading to the orientation signals and high f_H. With moving to the center, as we all know, it is difficult to form oriented crystals. However, for neat iPP and blends with low aPP content, such as A0, A10, and A20, strong orientation SAXS signals are observed in their core layers (Figure 5a–c), while at the same position, WAXD patterns show almost isotropic diffraction rings (Figure 2a–c). Because the SAXS patterns reflect the orientation degree of lamellae along the flow direction. The different results of the

dx.doi.org/10.1021/sc400140y | ACS Sustainable Chem. Eng. 2013, 1, 937–949

two characterization methods may be attributed to different scales.

With an increase in aPP content, the lamellar orientation (Figures 5 and 6) becomes weak at the fixed position of injection-molded parts, in accordance with the WAXD results (Figure 2), further proving the adverse effect of aPP on the formation of an oriented structure in aPP/iPP injection-molded parts. For A10, the strong intensity streak normal to the flow direction may be the result of the relative big electron density difference between aPP and oriented iPP crystals. When aPP content is above 50 wt %, the samples (A50 and A70) display significantly different SAXS patterns with low orientation signals almost in every layer of injection-molded parts (Figure 4d,e). The f_H of samples with high aPP content obtained from SAXS patterns are shown in Figure 6. The f_H of A50 and A70 is only about 0.18 and 0.11 in the skin layer, respectively, and decrease to almost 0 in the core layer, indicating completely isotropic structures in the core layers of aPP/iPP injection-molded parts with high aPP content. The isotropic SAXS patterns and low f_H of samples with high aPP content should be ascribed to the phase inversion of aPP/iPP blends, and in this case, iPP spherulites disperse uniformly in aPP matrix.

Using Bragg's law, the long spacing (L), reflecting the thickness of lamellar and amorphous region between two lamellae, is shown in Figure 7. It is shown that the long spacing

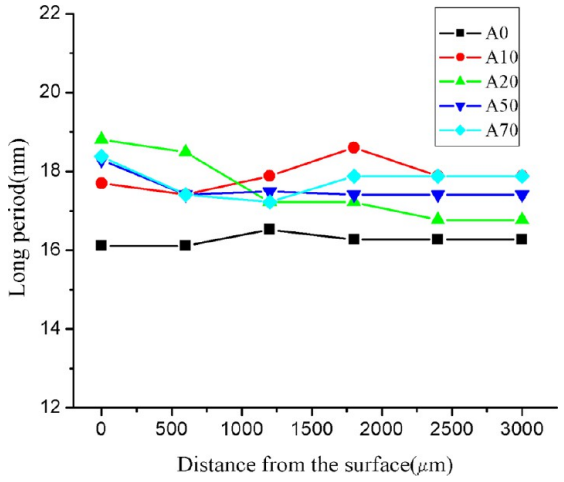

Figure 7. Long period of samples with different aPP contents along the direction perpendicular to flow direction.

of aPP/iPP blends with different aPP contents is almost independent of position in the injection-molded parts and shows only a slight increase, about 1−2 nm, compared to the neat iPP (i.e., A0 in Figure 7), demonstrating that only a small amount of aPP component inserts into the amorphous regions between iPP lamellae. The interfibrillar segregation (segregation within the spherulite) of aPP appears to be a dominant feature of the crystalline morphology of aPP/iPP blends, with only very modest interlamellar inclusion.

Thermal Behavior. The DSC melting results of the injection-molded aPP/iPP blends are presented in Table 1. The moderate variation of melting peak temperature (T_{mp}) with different aPP contents and positions in injection-molded part suggests the melting of α-iPP. Furthermore, with an increasing aPP content, a decrease in the melting peak temperature can be detected, indicating that the integrity of iPP crystals is somewhat disturbed due to the insertion of aPP

Table 1. DSC Results of Samples with Different App Contents

sample	layer	crystallinity	melting peak temperature (T_{mp})
A0	skin	35.0	166.1
	intermediate	34.4	166.6
	core	33.5	164.1
A10	skin	33.5	167.6
	intermediate	36.4	166.3
	core	36.6	166.2
A30	skin	36.3	166.0
	intermediate	37.5	166.8
	core	38.7	165.7
A50	skin	38.7	164.9
	intermediate	38.9	164.8
	core	38.1	165.0
A70	skin	34.9	163.0
	intermediate	34.9	163.0
	core	33.4	163.5

into the amorphous regions between iPP lamellae as confirmed by an increase in long spacing as shown in Figure 7. Furthermore, it is worth mentioning that a phenomenon of double melting peaks is detected for the skin layer of A10 (Figure 8), corresponding to the melting of shish-kebab structures, which also verifies the formation of oriented iPP crystals.[19,20]

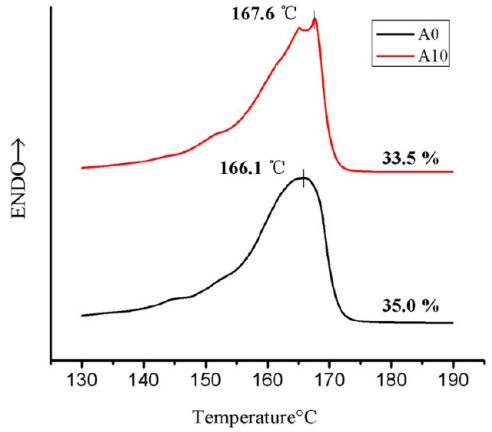

Figure 8. Selected DSC heating curves of skin layers of A0 and A10. T_{mp} and crystallinity of iPP are labeled.

The crystallinity (X_c) is shown in Table 1. It is shown that the X_c of blends is higher than that of neat iPP (A0) when the aPP content is lower than 50 wt %. For example, the X_c is 35.0%, 34.4%, and 33.5% in the skin, intermediate, and core layers of neat iPP, respectively, while it is 36.3%, 37.5%, and 38.7% in the same positions of the A30 sample, respectively, indicating that aPP molecular chains facilitate the diffusion of iPP chains and the growth of iPP crystals. As we know, a high crystallinity is helpful for the enhancement of mechanical properties of the injection-molded part, especially for the strength and stiffness. However, the content of crystals decreases gradually with the addition of an amorphous aPP component. The real content of crystals is only 32.9% in the core layer of A10 because the crystallizable iPP component is only 90 wt %. The decrease in crystal content may lead to the degradation of mechanical properties, especially strength and stiffness.

dx.doi.org/10.1021/sc400140y | ACS Sustainable Chem. Eng. 2013, 1, 937−949

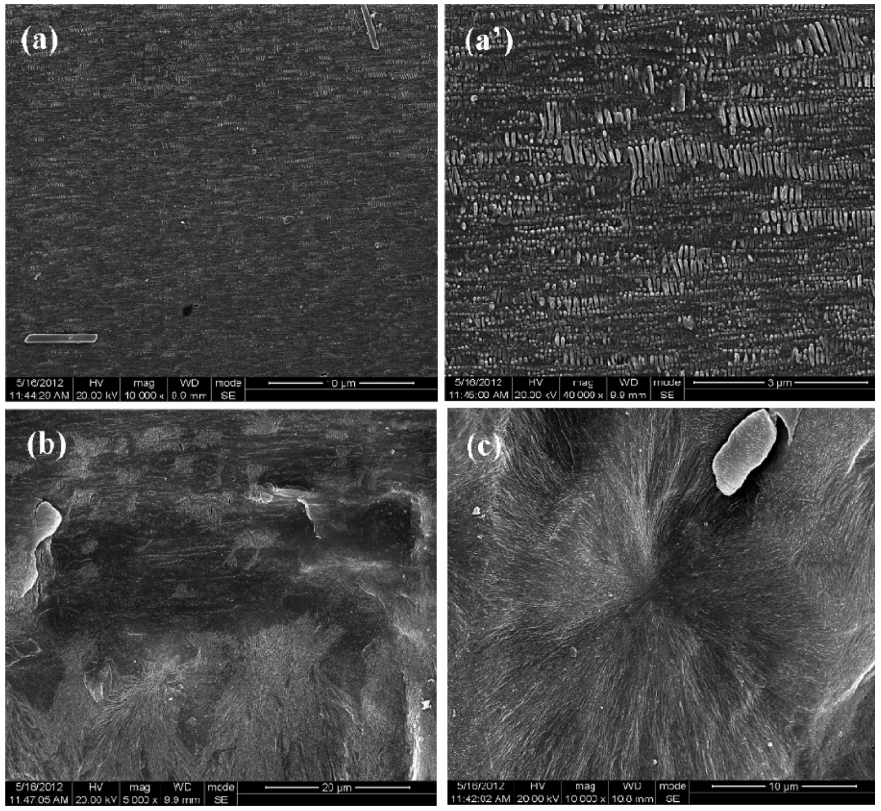

Figure 9. SEM micrographs of different layers of A0 after etched (a) skin layer, (b) intermediate layer, (c) core layer. (a′) is the magnified image of (a). The flow direction is horizontal.

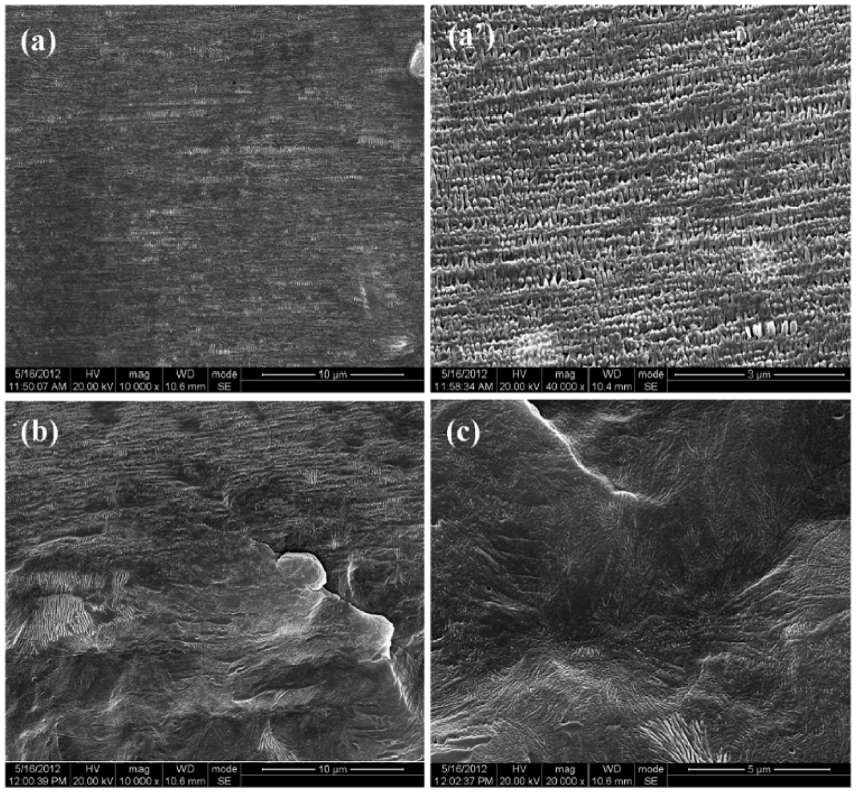

Figure 10. SEM micrographs of different layers of A10 after etched (a) skin layer, (b) intermediate layer, and (c) core layer. (a′) is the magnified image of (a). The flow direction is horizontal.

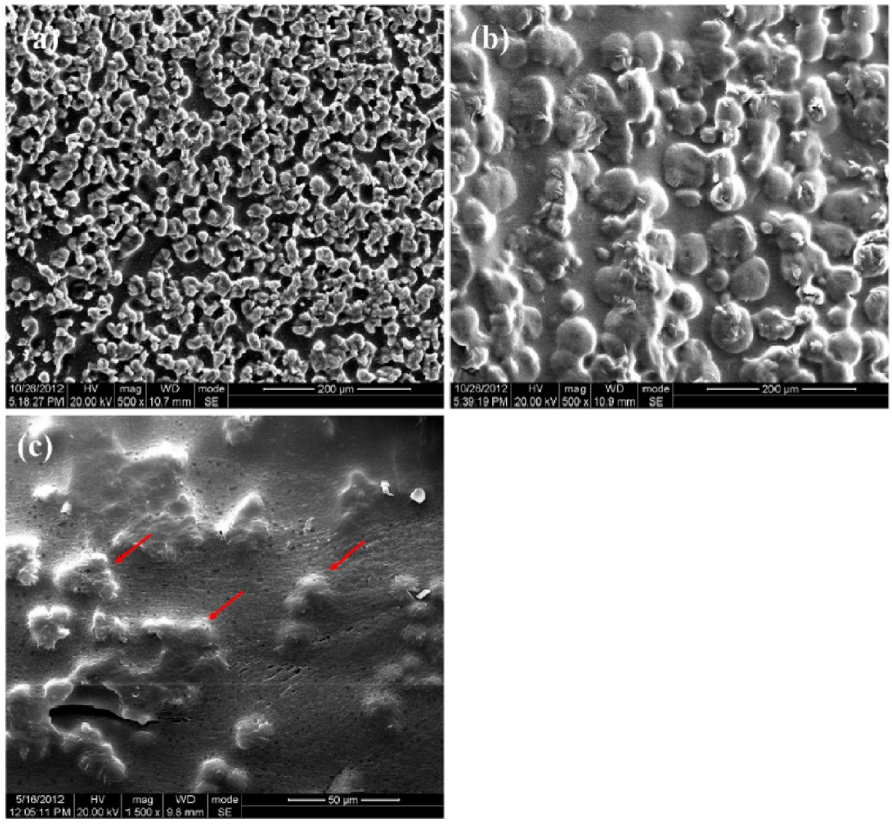

Figure 11. SEM micrographs, taken from the core layer of injection-molded parts, of the crystalline phase of iPP (some are indicated by arrows) in samples (a) A30, (b) A50, and (c) A70.

Crystalline Phase Morphology. Figure 9 shows the crystalline morphology of neat iPP sample. It displays oriented crystals (i.e., shish-kebab) in the skin and intermediate layers, while typical spherulites in the core layer, which is good agreement with the WAXD and SAXS results. With the distance varying from the surface to the center of injection-molded part, a change of crystal morphology from a dense shish-kebab structure (Figure 9a,a′) to spherulites (Figure 9c) is shown due to a gradually decreasing shear rate. Figure 9b shows the transitional region from oriented crystals to spherulites.

The crystalline phase morphology of sample A10, a typical example of aPP/iPP blends with low aPP content, is shown in Figure 10. Oriented crystals, i.e., shish-kebab structure, are observed in the skin layer of injection-molded parts (Figure 10a,a′). The transition region is shown in Figure 10b, which displays the coexistence of oriented crystals and spherulites. In the center of the injection-molded part, the structure changes from oriented crystals to typical isotropic spherulites (Figure 10c).

Otherwise, for the blend with a small amount of aPP component, the crystal phase morphology distribution of iPP in the blend is similar to the neat iPP sample. However, there are indeed some delicate differences between them. As shown in Figure 10a′, there are some void intervals between two shish-kebabs in sample A10, while the shish-kebabs in A0 are much denser (Figure 9a′). The apparent voids in A10 are caused by etched amorphous aPP existing between shish-kebabs. In the work reported by Lohse et al., after the aPP was removed from the aPP/iPP blend with hexane, they found that as the content of aPP in the blend increased the visibility of spherulites also increased.[18] The structure in sample A10 is in agreement with our speculation that aPP exists in the amorphous regions between iPP lamellae when aPP content is low. The integrity of the iPP crystal network, i.e., iPP crystalline regions together with chain entanglements can contact or interlink with each other as Bicakci et al. proposed in the blend of PEEK and PEI,[21] that is, the main stress transmission mesh is well kept.

Crystalline phase morphologies of aPP/iPP blends with aPP contents higher than 10 wt % are shown in Figure 11. Only the SEM micrographs taken from the core layers are shown due to the relatively homogeneous inner structure of the injection-molded parts with high aPP content. When the aPP content in the aPP/iPP blends rises to 30 wt %, iPP crystals still remain in the integrated crystal network but are disturbed by the aPP component as shown in Figure 11a. The iPP spherulites are separated by aPP phase that is exhibited by the void cavity in SEM micrographs due to its amorphous characteristic and easy etching, indicating the beginning of phase inversion and the gradual formation of aPP continuous phase. When the aPP content reaches 50 wt %, the co-continuous phase structure is observed in Figure 11b. With the aPP content up to 70 wt %, aPP phase becomes continuous, and unoriented iPP crystals disperse in aPP matrix and act like inorganic particles (Figure 10c), denoting that the phase inversion finished. It is in line with f_H results shown in Figure 6 that the highest f_H of A70 is only 0.11 and the f_H is close to 0 (ca. 0.01) indicating an isotropic inner structure of injection-molded parts. Under this condition, the iPP crystals cannot form an integrated crystal network, which may result in a severe decrease in mechanical properties of the injection-molded part.

dx.doi.org/10.1021/sc400140y | ACS Sustainable Chem. Eng. 2013, 1, 937−949

Mechanical Properties. Figure 12 illustrates the stress–strain curves of injection-molded aPP/iPP blends. All samples

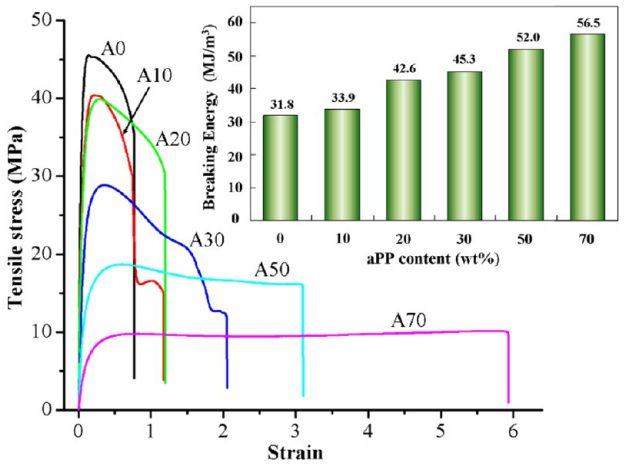

Figure 12. Selective stress–strain curves with the area under the stress–strain curve listed in the inset.

display a similar ductile tensile behavior with obvious yield and necking. With an increase in aPP content, the elongation at break increases while the tensile strength decreases. Using the area under the stress–strain curve, the energy absorbed during drawing was acquired, as illustrated in the inset of Figure 12, which indicates the breaking energy.[22] The breaking energy of aPP/iPP samples gradually rises with an increase in aPP content, where the A70 sample shows the highest toughness (56.5 MJ/m^3), about 78% higher than that of neat iPP, indicating an increase in ductility of aPP/iPP blends. In general, the toughness and ductility of iPP can be enhanced by the addition of aPP component but along with a decrease in strength and stiffness.[3,12] This allows us to believe that the processing method used in our work is feasible to toughen iPP with aPP at ambient temperature and above.

The specific values of tensile strength and elongation at break of all samples are summarized in Figure 13. Under low aPP contents (A10 and A20), the tensile strength (40.5 MPa) only shows a slight decrease compared to the pure iPP (45.9 MPa). Meanwhile, the breaking energy of aPP/iPP blends increases from 31.8 MJ/m^3 for neat iPP to 33.9 and 42.6 MJ/m^3 for A10 and A20, respectively (Figure 12). The reason is that when aPP content is lower than 20 wt %, the network of iPP crystals is still integral (Figure 10), and meantime, there are plenty of shish-kebabs in the skin layer of the blends (Figure 5d) and the relative crystallinity of iPP (Figure 8d) is high. Therefore, the strength of aPP/iPP is able to stay at the same level as the neat iPP sample. The mechanical properties of the injection-molded part declines notably when aPP content reaches 30 wt %. This is because the iPP crystal network (Figure 11a) has been disturbed by the aPP component, which breaks up the stress transmission mesh. At higher aPP content, for example, A50, the toughness is enhanced to 52.0 MJ/m^3, simultaneously the tensile strength stays at the level of 20 MPa and is in an accepted range. This mainly resulted from the change of continuous phase from crystallizable iPP to amorphous aPP. As the aPP content increases to 70 wt %, the tensile strength of the aPP/iPP blend decreases to about 10 MPa but with the highest toughness among all samples. In this case, phase inversion has completed, and aPP becomes continuous phase (Figure 11c), resulting in high ductility, especially the elongation at break, of

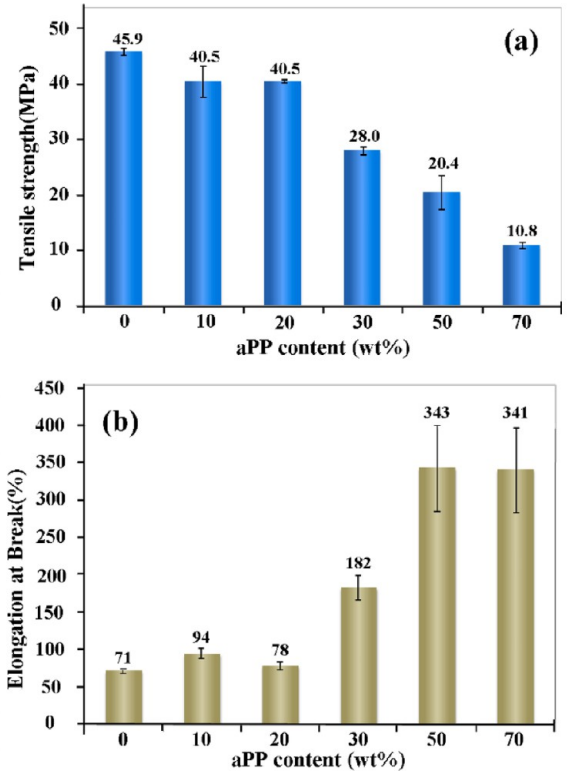

Figure 13. Mechanical properties of iPP/aPP blends with different aPP contents: (a) tensile strength and (b) elongation at break.

aPP/iPP blends. Nevertheless, the tensile strength of A70 (10.8 MPa) is obviously reduced because with a further increase in aPP content, the absolute content of the iPP crystal, the primary source of strength and stiffness of aPP/iPP blend, decreases. Compared to the results obtained by Wenig et al., the yield stress of the aPP/iPP blend film, predrawn under the flow gradient of 10^4 s^{-1}, was about 30 MPa with a 10 wt % aPP content.[13] However, using our processing method, i.e., a hot runner mold with big-sized gate, high melt temperature, and long packing time, the tensile strength of the injection-molded part is 40.5 MPa under the same aPP content. Therefore, the aPP/iPP blends with high mechanical properties owing to the optimized inner structure can be obtained through the suitable processing method.

In addition, within the whole range of the aPP content used in this work, the aPP/iPP blends undergo three stages of evolution of mechanical properties corresponding to the phase and crystalline morphology. It is also interesting to mention that when aPP content exceeds 20 wt %, the mechanical properties of the aPP/iPP blends change drastically, acting like percolation phenomenon in electro-conductive polymer composites, which results from the phase inversion.

DISCUSSION

The results reported above indicate that aPP/iPP blends with good mechanical properties have been obtained by utilizing a hot runner mold and long packing time during the injection-molding processing. The improved mechanical properties are closely related to the inner structures of injection-molded parts, which demonstrates that the mechanical properties of aPP/iPP blends can be divided into three stages of evolution with increasing aPP content.

Reasonable Mechanical Properties through Proper Processing. It has been well established that oriented iPP crystals (i.e., shish-kebabs) can bring about notable reinforcement on iPP products. The shish-kebab structure, induced by shear flow in the industrial processing (e.g., extrusion, injection molding, spinning), have attracted much attention due to the significant theoretical values and practical applications. According to previous studies, oriented chains[23] or networks[24−26] are necessary for the formation of shish-kebab structures. However, just as reported by Carlson et al., the oriented chains under flow tend to relax back to their random configuration after cessation of large-amplitude shear strain.[1] In our case, the relaxation process of the oriented chains or networks is accelerated by the addition of aPP because the short chains of aPP are beneficial for the mobility of iPP molecules, which inhibits the formation of oriented crystals like shish-kebab in aPP/iPP blends.

To verify whether the addition of aPP will hinder the orientation of iPP molecular chains after shear flow, a polarized optical microscope (POM) with shear stage was applied to observe the crystallization process of aPP/iPP blends and neat iPP. Under quiescent crystallization condition (i.e., without shear flow) at 141 °C for 50 min, a few spherulites were observed in neat iPP (Figure 14a). After a flow field was applied, the crystallization process was obviously accelerated, and oriented cylindrical crystals appeared (Figure 14b). However, when 10 wt % aPP was added into iPP, no spherulites appeared under quiescent crystallization condition in Figure 14c, even under the shear condition of $\dot{\gamma} = 10\ s^{-1}$ and $t_s = 30$ s, which induces oriented cylindrical crystals in neat iPP melt as mentioned above, indicating that aPP is disadvantageous to the nucleation of iPP melt and further to the formation of oriented structures like shish-kebabs and cylindrical crystals. This result is in agreement with the result of WAXD (Crystalline Structure section), and SAXS (Oriented Structure section), i.e., the formation of oriented iPP crystals becomes more and more difficult with an increase in aPP content.

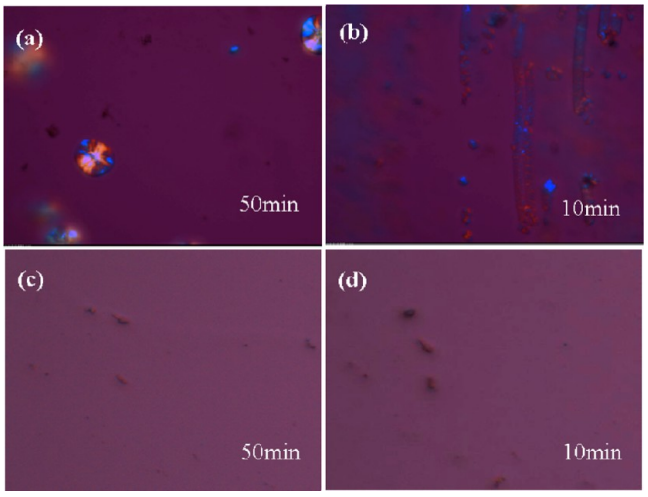

Figure 14. POM micrographs of neat iPP [(a) and (b)] and blend with 10 wt % aPP [(c) and (d)] at different crystallization conditions: (a) and (c) 141 °C under quiescent conditions; (b) and (d) 141 °C after shearing at $\dot{\gamma} = 10\ s^{-1}$ for $t_s = 30$s.

However, in our work, shish-kebab structure (Figures 9 and 10) were obtained in the skin and intermediate layers of injection-molded blend parts, especially with low aPP content. The special processing condition, i.e., large-sized gate of mold, long packing time, and high melt temperature, leads to a long packing process so that more melt can be filled into the mold cavity to compensate the shrinkage of melt. Therefore, the melt closer to the center of the sample can undergo the microflow caused by packing and further is induced to form more shish-kebabs. Thus, the shish-kebabs in the skin and intermediate layers of the sample with low aPP content make a difference to the mechanical properties and offset the decline in strength due to the addition of aPP to some extent.

As we know, high crystallinity is also helpful for the enhancement of mechanical properties of the injection-molded part, especially for the strength and stiffness. Until now, the influence of aPP on the crystallinity of iPP is still in debate. Chen et al. reported that a small amount of aPP could lead to an increase in crystallinity in aPP/iPP blends, while the opposite is the case when aPP content is high.[27] Wang et al. achieved similar results that up to 60 wt % aPP there were few changes in the induction time and the half-time, whereas when aPP content reached 80 wt %, the crystallization kinetics showed a significant delay, which may result in relatively low crystallinity.[9] However, Na et al. found that the onset crystallization temperature of aPP/iPP blends shifted by about 5 °C toward higher temperature, demonstrating that the nucleation ability was enhanced,[28] which may lead to higher crystallinity under the same condition. According to the above results, the variation of mechanical properties of aPP/iPP blends with different aPP contents cannot be conjectured due to the indeterminacy effect of aPP on the crystallinity of iPP. Under this circumstance, we carried out nonisothermal crystallization of aPP/iPP blends to confirm the influence of aPP on the crystallinity of iPP definitely.

The DSC results in Figure 15 and POM micrographs in Figure 14 confirmed that the addition of aPP obviously inhibited the nucleation and growth of iPP. The onset crystallization temperature shifted by nearly 15 °C toward lower temperatures for sample A70, demonstrating that the nucleation ability of iPP was lowered. From our DSC results, we conclude without doubt that aPP would suppress the crystallization of iPP under all aPP contents employed in our

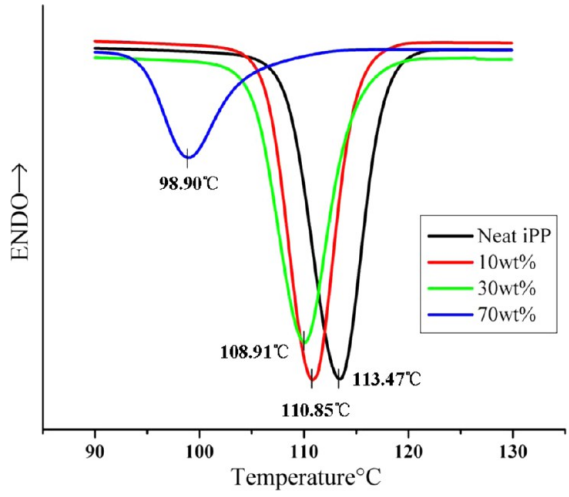

Figure 15. Nonisothermal crystallization diagrams of samples A0, A10, A30, and A70.

dx.doi.org/10.1021/sc400140y | ACS Sustainable Chem. Eng. 2013, 1, 937−949

experiment, which may cause the decline of crystallinity of iPP in the injection-molded part.

However, in our experiment, a hot runner with high melt temperature is favored for the crystallization of iPP. Meanwhile, slow cooling leads to long packing time in the injection cycle and guarantees enough time for iPP to crystallize completely. For these reasons, the crystallinity of iPP in aPP/iPP blends does not decline dramatically compared to neat iPP, even with some enhancement, as shown in Table 1. The relatively high crystallinity of iPP can compensate, to some extent, the reduction of mechanical properties of aPP/iPP blends caused by the addition of aPP. Then, the addition of aPP, promoting the liquidity of melts during the filling and packing stages, as well as long packing time, resulted in dense inner structure, which also makes for good mechanical properties of aPP/iPP blends. In addition, the formation of shish-kebab structures in skin layers of samples with low aPP content as shown in Figure 10, i.e., A10 and A20, are in favor of good mechanical properties to a certain degree. Overall, all aPP/iPP blends with good mechanical properties have been achieved by utilizing a hot runner mold with a big-sized gate resulting in high melt temperature and long packing time.

Percolation Phenomenon in Mechanical Properties. As to the evolution of mechanical properties of the injection-molded part with an increase in aPP content, it can be understood from the inner structure. With low aPP content, i.e., A10 and A20, iPP crystals can keep an integrated network, i.e., interlinked in the whole injection-molded part, as shown in Figure 10. This result is similar to the physical network with oriented crystallites raised by Bicakci and Cakmak in a stretched PEI/PEEK blend that is also a kind of crystallizable/noncrystallizable blend.[21] The high rigidity of the crystalline domains and entangled chains, together with the crystal networks, can bear most external stress during tensile test. Furthermore, the formation of shish-kebab structures in the skin layers of samples, confirmed by SEM micrographs (Figure 10a,a′), offset a decrease in tensile strength with the addition of aPP. So the mechanical properties of aPP/iPP blends are not notably reduced by the addition of aPP compared to pure iPP.

Whereas, with a further increase in aPP content, phase inversion starts to happen and iPP crystal networks become broken due to the large amount of the aPP amorphous phase, leading to notable changes in mechanical properties of the blend, acting like percolation phenomenon in electro-conductive polymer composites. With aPP content changing from 30 to 50 wt %, the integrated iPP crystals network turned into a co-continuous phase structure, as shown in Figure 11a. As a result, the mechanical properties of aPP/iPP blends are altered by aPP component with the gradual formation of a new aPP matrix leading to the percolation phenomenon in mechanical properties.

When aPP content exceeds 50 wt %, phase inversion has completed, and aPP becomes a continuous phase. In the meantime, separated iPP spherulites disperse in the aPP matrix like inorganic fillers, resulting in isotropic signals in both WAXD and SAXS patterns (Figures 2d,e and 5d,e) and low f_H (Figure 6). The SEM micrographs of A70 proved the hypothesis above (Figure 11c). Therefore, the deformation of the injection-molded part mainly comes from the extension of the aPP continuous phase. With increasing the aPP content further, the elongation at break of aPP/iPP blends will not change obviously (Figure 13b) because the inner structure of the injection-molded part will not change essentially. However, the tensile strength and modulus are further reduced by the addition of more aPP because the absolute content of separated iPP spherulites in aPP matrix decreases continuously.

Furthermore, there are no conjoint molecular chains to link separated iPP spherulites and aPP matrix; thus, the iPP crystal phase cannot act as physical cross-link point. As a result, aPP/iPP blends have no resilience and possesses relatively poor properties compared to other elastomeric materials. Thus, with high aPP content, the final mechanical properties of aPP/iPP blends are not totally satisfactory, even with high ductility. Further explorations are needed to solve these problems.

CONCLUSION

In this work, aPP/iPP blends with high toughness and desired tensile strength were successfully prepared by using suitable processing conditions, i.e., a hot runner mold with big-sized gate, high melting temperature, and long packing time, which all are in favor of the crystallization of iPP. This overturns the traditional view that aPP will suppress the nucleation and crystallization of iPP in aPP/iPP blends and goes against the formation of shish-kebab under a flow field of injection molding. Our results open a new field for the usage of aPP, the byproduct of iPP production, on a large scale.

The mechanical properties of aPP/iPP blends can be divided into three stages of evolution with an increase in aPP content. When the aPP content is lower than 20 wt %, the mechanical properties of aPP/iPP blends change just a little compared to neat iPP because the networks of the iPP crystal still stay integral and are able to transfer outer stress. When aPP content is higher than 20 wt %, phase transition begins, and the crystal network of iPP is destroyed. Thus, the mechanical properties of the aPP/iPP blend changed dramatically, acting like the percolation phenomenon in conductive polymer composites. Further increasing the aPP content completes the phase transition, and aPP becomes a continuous phase. Hence, more aPP will not affect the mechanical properties of the aPP/iPP blend observably again.

AUTHOR INFORMATION

Corresponding Author

*E-mail: leijun@scu.edu.cn (J.L.); zmli@scu.edu.cn (Z.-M.L.).

Notes

The authors declare no competing financial interest.

ACKNOWLEDGMENTS

This work was supported by National Natural Science Foundation of China (U1162131, 51121001, 21276168, and 51273131).

REFERENCES

(1) Carlson, E. D; Fuller, G. G.; Waymouth, R. M. Transient birefringence of elastomeric polypropylene subjected to step shear strain. *Macromolecules* **1999**, *32*, 8094−8099.

(2) Haylock, J. C.; Phillips, R. A.; Wolkowicz, M. D. In *Metallocene-Based Polyolefins: Preparation, Properties, and Technology*; Scheirs, J.; Kaminsky, W., Eds.; Wiley: Chichester, England, 2000; Vol. 2, pp 333−363.

(3) Friedrich, K. Strength and fracture of crystalline isotactic polypropylene and the effect of molecular and morphological parameters. *Prog. Colloid Polym. Sci.* **1979**, *66*, 299−309.

(4) Lohse, D. J. The melt compatibility of blends of polypropylene and ethylene-propylene copolymers. *Polym. Eng. Sci.* **1986**, *26*, 1500−1509.
(5) Maier, R. D.; Thomann, R.; Kressler, J.; Mulhaupt, R.; Rudolf, B. The influence of stereoregularity on the miscibility of poly(propylene)s. *J. Polym. Sci., Part B: Polym. Phys.* **1997**, *35*, 1135−1144.
(6) Keith, H. D.; Padden, F. J. Spherulitic crystallization from the melt. II. Influence of fractionation and impurity segregation on the kinetics of crystallization. *J. Appl. Phys.* **1964**, *35*, 1286.
(7) Choi, P.; Mattice, W. L. Molecular origin of demixing, prior to crystallization, of atactic polypropylene/isotactic polypropylene blends upon cooling from the melt. *J. Chem. Phys.* **2004**, *121*, 8647−8651.
(8) Phillips, R. A. Macromorphology of polypropylene homopolymer tacticity mixtures. *J. Polym. Sci., Part B: Polym. Phys.* **2000**, *38*, 1947−1964.
(9) Wang, Z. G.; Phillips, R. A.; Hsiao, B. S. Morphology development during isothermal crystallization. I. Isotactic and atactic polypropylene blends. *J. Polym. Sci., Part B: Polym. Phys.* **2000**, *38*, 2580−2590.
(10) Keith, H. D.; Padden, F. J. Spherulitic crystallization from the melt. I. Fractionation and impurity segregation and their influence on crystalline morphology. *J. Appl. Phys.* **1964**, *35*, 1270.
(11) Lustiger, A.; Marzinsky, C. N.; Mueller, R. R. Spherulite boundary strengthening concept for toughening polypropylene. *J. Polym. Sci., Part B: Polym. Phys.* **1998**, *36*, 2047−2056.
(12) Wenig, W.; Schöller, T. Transfer of load from matrix to fiber in self-reinforced polymer composites. *Colloid Polym. Sci.* **1991**, *269*, 1212−1223.
(13) Cheng, S. Z. D.; Janimak, J. J.; Zhang, A.; Cheng, H. N. Regime transitions in fractions of isotactic polypropylene. *Macromolecules* **1990**, *23*, 298−303.
(14) Chen, Y. H.; Zhong, G. J.; Wang, Y.; Li, Z. M.; Li, L. B. Unusual tuning of mechanical properties of isotactic polypropylene using counteraction of shear flow and β-nucleating agent on β-form nucleation. *Macromolecules* **2009**, *42*, 4343−4348.
(15) Olley, R. H.; Bassett, D. C. An improved permanganic etchant for polyolefines. *Polymer* **1982**, *23*, 1707−1710.
(16) Somani, R. H.; Yang, L.; Hsiao, B. S.; Fruitwala, H. Nature of shear-induced primary nuclei in iPP melt. *J. Macromol. Sci., Part B: Phys* **2003**, *B42*, 515−531.
(17) J. Varga, J. Karger-Kocsis: Rules of supermolecular structure formation in sheared isotactic polypropylene melts. *J. Polymer Sci. Part B: Polym. Phys.* **1996**, *34*, 657−670.
(18) Lohse, D. J.; Wissler, G. E. Compatibility and morphology of blends of isotactic and atactic polypropylene. *J. Mater. Sci.* **1991**, *26*, 743−748.
(19) Cao, W.; Wang, K.; Zhang, Q.; Du, R. N.; Fu, Q. The hierarchy structure and orientation of high density polyethylene obtained via dynamic packing injection molding. *Polymer* **2006**, *47*, 6857−6867.
(20) Liang, S.; Wang, K.; Tang, C. Y.; Zhang, Q.; Du, R. N.; Fu, Q. Unexpected molecular weight dependence of shish-kebab structure in the oriented linear low density polyethylene/high density polyethylene blends. *J. Chem. Phys.* **2008**, *128*, 174902.
(21) Bicakci, S.; Cakmak, M. Kinetics of rapid structural changes during heat setting of preoriented PEEK/PEI blend films as followed by spectral birefringence technique. *Polymer.* **2002**, *43*, 2737−2746.
(22) Xu, H.; Zhong, G. J.; Fu, Q.; Lei, J.; Jiang, W.; Hsiao, B. S.; Li, Z. M. Formation of shish-kebabs in injection-molded poly(L-lactic acid) by Application of an intense flow field. *ACS Appl. Mater. Interfaces* **2012**, *4*, 6774−6784.
(23) Keller, A.; Kolnaar, H.W. H. *Flow Induced Orientation and Structure Formation*; VCH: New York, 1997; Vol. *18*.
(24) Hsiao, B. S.; Yang, L.; Somani, R. H.; Avila-Orta, C. A.; Zhu, L. Unexpected shish-kebab structure in a sheared polyethylene melt. *Phys. Rev. Lett.* **2005**, *94*, 117802.
(25) Zhao, B. J.; Li, X. Y.; Huang, Y. J.; Cong, Y. H.; Ma, Z.; Shao, C. G.; An, H. N.; Yan, T. Z.; Li, L. B. Inducing crystallization of polymer through stretched network. *Macromolecules* **2009**, *42*, 1428−1432.
(26) Yang, H. R.; Lei, J.; Li, L. B.; Fu, Q.; Li, Z. M. Formation of interlinked shish-kebabs in injection-molded polyethylene under the coexistence of lightly cross-linked chain network and oscillation shear flow. *Macromolecules* **2012**, *45*, 6600−6610.
(27) Chen, J. H.; Chang, Y. L. Isothermal crystallization kinetics and morphology development of isotactic polypropylene blends with atactic polypropylene. *J. Appl. Polym. Sci.* **2007**, *103*, 1093−1104.
(28) Na, B.; Guo, M.; Yang, J. H.; Tan, H.; Zhang, Q.; Fu, Q. Crystal morphology and transcrystallization mechanism of isotactic polypropylene induced by fibres: Interface nucleation versus bulk nucleation. *Polym. Int.* **2006**, *55*, 441−448.